

Article

Organic and Inorganic Hybrid Composite Phase Change Material for Inhibiting the Thermal Runaway of Lithium-Ion Batteries

Jie Mei ^{1,2}, Guoqing Shi ^{1,2,*}, He Liu ^{1,2} and Zhi Wang ^{1,2}

¹ College of Safety Engineering, China University of Mining and Technology, Xuzhou 221116, China; jmei@cumt.edu.cn (J.M.); liuhe@cumt.edu.cn (H.L.); zhiwang@cumt.edu.cn (Z.W.)

² State Key Laboratory of Coal Resources and Safe Mining, China University of Mining and Technology, Xuzhou 221116, China

* Correspondence: sgq@cumt.edu.cn

Abstract: To deal with the flammability of PA (paraffin), this paper proposes a CPCM (composite phase change material) with a high heat-absorbing capacity for mitigating the thermal runaway of lithium-ion batteries. Two heating power levels were used to trigger thermal runaway in order to investigate the influence of heating power on thermal runaway characteristics and the mitigation effect of the PCM (phase change material). Thermal runaway processes and temperature changes were recorded. The results showed that heating results in a violent reaction of the battery, generating a high temperature and a bright flame, and the burning of PA increases the duration of a steady flame, indicating an increased threat. SA (sodium acetate trihydrate) effectively inhibited PA combustion, and the combustion time was reduced by 40.5%. PA/SA effectively retarded the rise in temperature of the battery, and the temperature rise rate was reduced by 87.3%. Increased heating power caused faster thermal runaway, and the thermal runaway mitigation effect of the CPCM was dramatically reduced. This study may provide a reference for the safe design and improvement of thermal management systems.

Keywords: lithium-ion battery; paraffin; thermal runaway; phase change material; heat absorption



Citation: Mei, J.; Shi, G.; Liu, H.; Wang, Z. Organic and Inorganic Hybrid Composite Phase Change Material for Inhibiting the Thermal Runaway of Lithium-Ion Batteries. *Batteries* **2023**, *9*, 513. <https://doi.org/10.3390/batteries9100513>

Academic Editors: Carlos Ziebert and Thomas Wetzel

Received: 11 September 2023

Revised: 10 October 2023

Accepted: 16 October 2023

Published: 17 October 2023



Copyright: © 2023 by the authors. Licensee MDPI, Basel, Switzerland. This article is an open access article distributed under the terms and conditions of the Creative Commons Attribution (CC BY) license (<https://creativecommons.org/licenses/by/4.0/>).

1. Introduction

Because of their high energy and power density, lithium-ion batteries have been used in a variety of applications in recent decades, including electric vehicles, large-scale energy storage, and power grids [1–3]. However, the long-term operation of batteries at a high temperature reduces their lifetime and may induce thermal runaway, leading to great danger [4–6]. As a result, the construction of a thermal management system for lithium-ion batteries has been proposed in order to assure the safety of the batteries [7–9].

PA (paraffin) is considered an ideal thermal management material for lithium-ion batteries due to its suitable phase change temperature, large latent heat and corrosion resistance. Abbas and An et al. respectively used PA as a PCM (phase change material) for the thermal management system of lithium-ion batteries and employed different liquid-cooled plates in combination with PA to form an efficient BTMS (battery thermal management system). The results showed that the heat-absorbing effect of PA suppressed the temperature rise of the batteries and gained a more homogeneous temperature distribution among the module, and the liquid-cooled plates further improved the thermal management performance of PA [10,11]. In order to improve the thermal management performance of PA, PA is blended with other materials to obtain improved properties, such as thermal conductivity, and this blend is called a composite phase change material. To address the low thermal conductivity of PA, Hussain et al. introduced PA into graphene-coated nickel and found that the thermal conductivity of the CPCM (composite phase change material) was significantly improved and the battery temperature was further reduced [12]. According to research conducted by Wang et al., a graphite powder/paraffin/nickel foam ternary CPCM

can not only regulate the temperature increase of the battery surface, but can also decrease the heat dissipation of the battery at low temperatures to assure normal usage [13]. Zhao et al. designed a BTMS with a combination of a copper foam/paraffin CPCM and liquid cooling channels, showing that the introduction of liquid cooling reduces the maximum temperature of the battery while also leading to a bigger temperature difference; thus, a balance between the maximum temperature and temperature uniformity is required [14]. Greco et al. employed compressed expanded natural graphite to increase the thermal conductivity of paraffin and demonstrated that the composite performed significantly better than forced air cooling [15]. Kang et al. introduced a new high thermal conductivity and insulating CPCM made of PA and silicon carbide for the thermal management of lithium-ion batteries and found that the temperature of the battery pack was significantly reduced [16]. Wang et al. investigated the effects of PA with different melting points and different mass fractions of EG (expandable graphite) on the thermal management performance of a CPCM using numerical simulation and the results showed that 48 °C was a suitable melting point, whereas the larger the mass fraction of EG, the higher the battery temperature [17]. Chen et al. used EG and silicon carbide as thermally conductive materials, blending them with PA to form a CPCM, and found that the thermal conductivity could reach up to 4.086 W/(m · K), exhibiting an extremely high cooling efficiency [18]. The battery temperature was lowest with 9 fins, according to Chen et al.'s investigation of the influence of the number of fins on the thermal management performance of paraffin [19]. Fins and expanded graphite can significantly improve the thermal management performance of paraffin, according to research by Mei et al. [20].

However, batteries may still experience thermal runaway due to aging, design flaws, and the presence of some extreme conditions. Liu et al. showed that lithium plating is generated during the charging and discharging of lithium-ion batteries, which is highly likely to lead to thermal runaway [21]. According to research by Liu et al., even slight overcharging can cause the battery's internal resistance to rise, which in turn causes the battery to heat up more, eventually leading to thermal runaway [22]. Further research on the thermal runaway caused by overcharging was conducted by Mao et al. The findings indicated that after overcharging, the deposited lithium reacts with the electrolyte to produce a significant amount of heat, and the stability of the cathode material also diminishes [23]. Hu et al. investigated the thermal runaway characteristics of electrical abuse and showed that with an increasing charge rate, the battery presents a higher thermal risk, with a lower onset temperature and higher maximum temperature [24]. Liu et al. investigated the thermal runaway of lithium-ion batteries under overcharging and showed that high-current overcharging results in two violent combustion-explosion reactions [25]. External heat sources are another frequent cause of thermal runaway in lithium-ion batteries, which not only produce a great deal of heat, but also result in the production of hazardous combustible and toxic gases [26–29]. Huang et al. investigated the effect of heating power on the thermal runaway of batteries, and the results showed that with the increase in heating power, the onset time advances and the heat release rate increases [30]. When Md Said et al. simulated the effects of the mechanical impact on lithium-ion batteries, they found that the battery was rapidly damaged and produced an extremely high temperature [31]. Therefore, even though the BTMS regulates the rise in battery temperature, thermal runaway may still occur, and it is necessary to investigate the impact of a PCM during thermal runaway. In the case of a battery's thermal runaway, PA, a flammable PCM, can increase the threat. Zhang et al. found that a composite phase change material consisting of paraffin and expanded graphite helps dissipate heat, but thermal runaway propagates more widely once it has occurred [32]. Dai et al. conducted thermal runaway experiments on a 18650 Li-ion battery containing PA and found that the heat-absorbing effect of PA prolongs the onset of thermal runaway, but its flammability greatly increases the heat release, and the use of a mixture of flame retardants can reduce the heat release rate [33]. Weng et al. showed that the addition of EG to PA significantly suppresses the combustion flame, but accelerates the propagation of thermal runaway [34].

Huang et al. used a composite flame retardant in combination with paraffin wax and other materials to form a new type of flame-retardant flexible CPCM and discovered that the addition of 15 wt% is able to inhibit heat diffusion and resist flames, achieving a better flame retardant effect [35]. Graphene-enhanced hybrids are effective at preventing the spread of thermal runaway, according to Wang et al. [36]. However, there are few detailed studies on the impact of PA on the thermal runaway of lithium-ion battery processes, and the use of a CPCM for inhibiting the flammability of PA and the thermal runaway threat is rarely investigated. In addition, the effect of different heating powers on thermal runaway and validation of the effectiveness of a CPCM have rarely been reported.

Therefore, in this paper, the inorganic material SA (sodium acetate trihydrate) was mixed with PA (paraffin) to form a CPCM, and its inhibitory effect on PA's flammability, as well as the effect on the thermal runaway of batteries, was investigated. Due to the high latent heat and non-flammability of SA, the evaporation of its water of crystallization absorbs heat, which theoretically inhibits the combustion of PA and reduces the threat of a battery's thermal runaway. Additionally, the effectiveness of the CPCM was evaluated at various heat intensities, and data on the thermal runaway process, flame, and battery temperature were gathered and analyzed. Some characteristic parameters such as the temperature rise rate, temperature rise time after thermal runaway, and peak battery temperature were compared and analyzed. This study serves as a guide for creating a secure PCM lithium-ion BTMS (battery temperature management system).

2. Experimental Section

2.1. Materials

The battery used in this study, a Sony US18650VTC5, had a 2600 mAh capacity, weighed approximately 45.4 g, and had discharge and charge cutoff voltages of 2.0 and 4.2 V, respectively. The positive electrode of the battery was nickel–manganese–cobalt ternary material and the negative electrode was graphite. Before testing, the battery was cycled three times, and was then fully charged to 100% SOC to show the greatest hazard of thermal runaway. The two PCMs used in this paper were PA and SA, and their detailed parameters are shown in Table 1. The PA was supplied by Henan Baihuali Chemical Product Co., Ltd., Zhengzhou, China, and its phase transition temperature was 48–50 °C, with a latent heat of 136 J/g. The SA was supplied by Sinopharm Chemical Reagent Co., Ltd., Shanghai, China, and its phase transition temperature was slightly higher than that of the PA at 58 °C, with a latent heat of 260 J/g, which was nearly twice as much as that of the PA. In addition, the SA contained crystal water, which can absorb a large amount of heat in the case of thermal runaway, thus lowering the battery temperature.

Table 1. Physical and thermochemical properties of the materials.

Name	Molecular Formula	$\rho/\text{g/cm}^3$	Melting Point/°C	Boiling Point/°C	Specific Heat Capacity (J/(kg·°C))
Paraffin SA	$\text{C}_n\text{H}_{2n+2}$ $\text{CH}_3\text{COONa}\cdot 3\text{H}_2\text{O}$	0.88 1.45	45–48 58	322 400	2140 1970

2.2. Experimental Setup

Figure 1 depicts a schematic of the experimental setup used to study thermal runaway. The heater was the same size as the battery and provided 200 and 500 W of heating power, respectively. The heater stopped heating after the battery suffered thermal runaway. The battery was placed in a battery tube made of an Mg–Al (magnesium–aluminum) alloy (type 5052) with a thermal conductivity of 138 W/m·°C, a diameter of 36 mm, a height of 65 mm, and a thickness of 2 mm. There were three screws (8 mm in diameter) on the top and bottom of the tube to hold the battery in place. To measure the temperature change during thermal runaway, thermocouples were placed in the middle of the battery surface, as well as 5 and 15 cm above the battery. The flame temperatures at 5 and 15 cm above

the battery were termed T_{f1} and T_{f2} , respectively, while the temperature at the battery surface was assigned the designation T_b . The SA and PA were placed up-and-down to maximize the heat absorption effect of the SA, with the SA occupying a third of the volume. The temperature of the material was denoted T_m . K-type thermocouples were utilized to measure the temperature, and C-7018 was used to record data. Digital cameras were used to record the thermal runaway process.

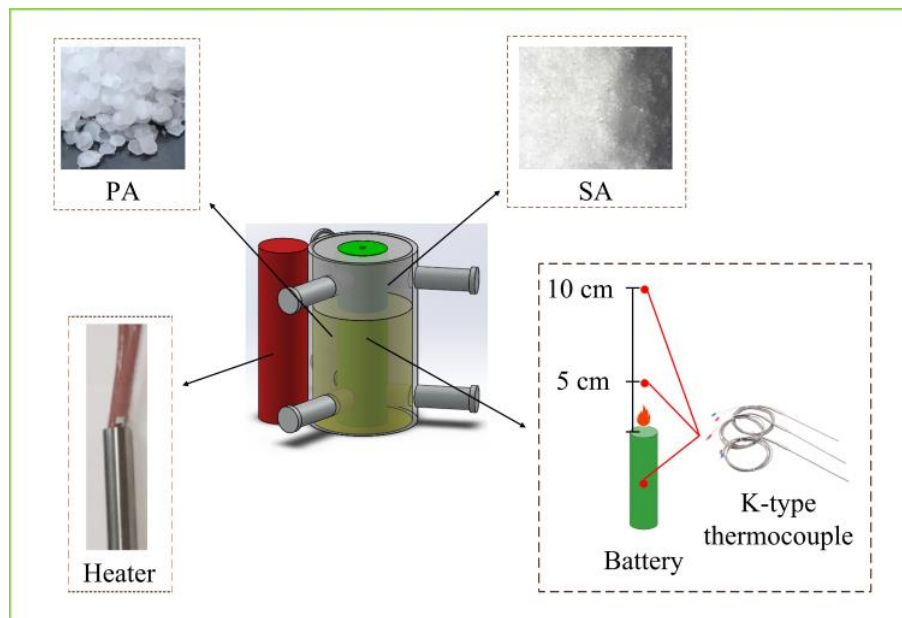


Figure 1. Schematic diagram of the experimental platform.

2.3. Experimental Conditions

The tests were categorized into three groups, i.e., Group I (single battery), Group II (PA), and Group III (SA/PA). Excluding the volume occupied by the fixation screws, the amount of PA added alone was 14.55 g, whereas the amount of PA and SA added to the CPCM was 9.7 and 7.99 g, respectively. The impact of heating power on the thermal runaway was examined using two heating powers, 200 and 500 W. Each test was performed at least three times and the relative standard deviations of characteristic parameters were calculated for all groups. A smaller relative standard deviation means more accurate experimental data. The standard deviations of the characteristic times and temperature during thermal runaway were less than 15%, so the experimental results are highly consistent and reliable.

3. Results and Discussions

3.1. Thermal Runaway Behaviors of a Single Battery

The thermal runaway process of a Group I with a single battery is depicted in Figure 2a, which can be divided into four stages: Heating, jet spark, steady flame, and extinguishing. It can be seen that the thermal runaway of the battery generated a great danger—jet sparks and flame combustion. The t_{com} (the duration of a stable combustion stage) of a single battery was 10 s, and the main burning substances were internal electrolyte and separator, alongside other combustible substances, with the combustion generating a great threat to the surrounding environment. According to Figure 2b, the battery suffered more severe damage following thermal runaway, as the top safety valve ruptured, and the battery case contained more carbon black as a result of combustion.

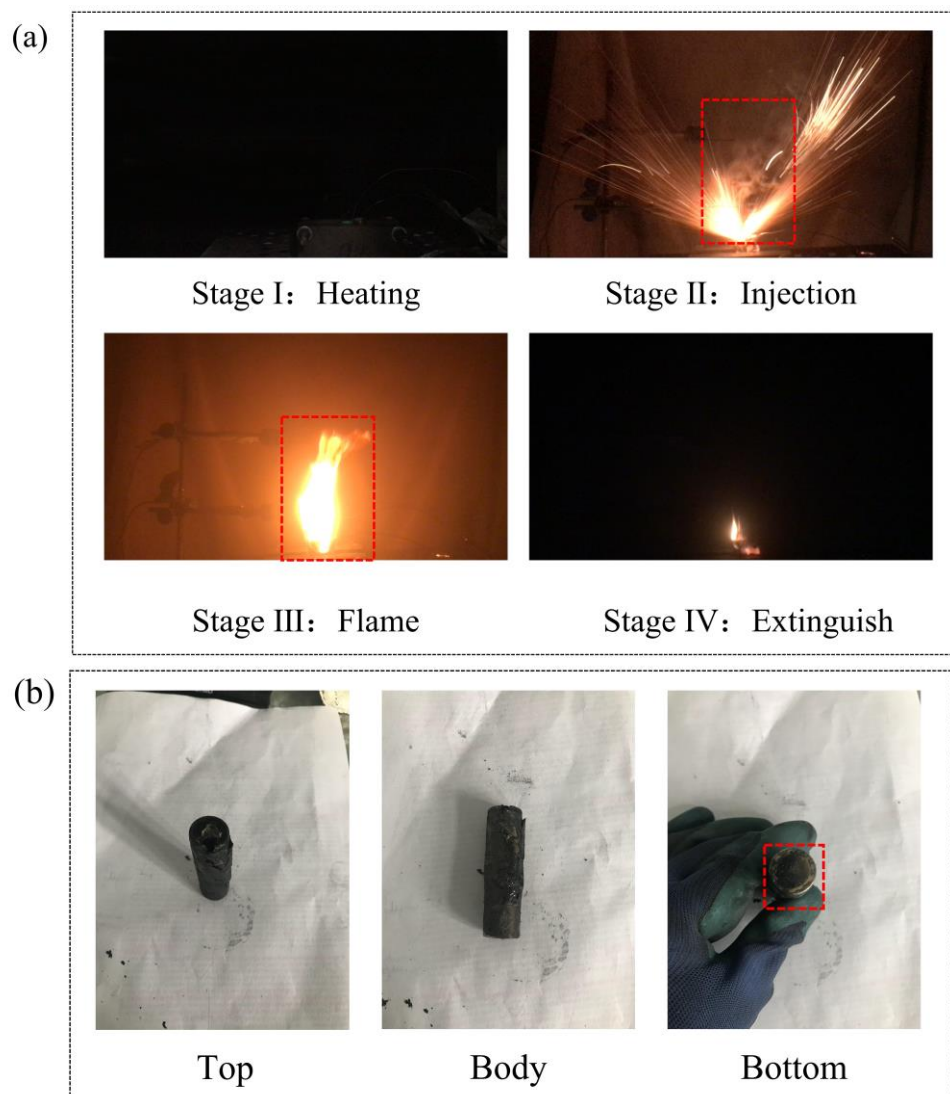


Figure 2. Single battery thermal runaway process and residues: (a) The thermal runaway process; (b) the residues.

As shown in Figure 3a, the battery heated up to $133.9\text{ }^{\circ}\text{C}$ after 393 s, at which point it entered the thermal runaway stage, causing a sudden rise in T_b , jet sparks, and a continuous flame. Around 432 s, T_b reached a peak value of $681.9\text{ }^{\circ}\text{C}$ and then decreased, indicating the ending of the thermal runaway. Due to the heater rod's constant heating, the battery experienced thermal runaway, which was characterized by an extraordinarily high temperature and a potentially dangerous flame. The $T_{f2-\max}$ (maximum value of T_{f2}) was $1031.9\text{ }^{\circ}\text{C}$, which was much higher than T_{f1} , indicating that the battery flame height was above 15 cm, which would cause serious damage to the surroundings and even a secondary disaster.

3.2. Effect of the PCMs on Thermal Runaway

The thermal runaway process and residues of the battery for Groups II (PA) and III (PA/SA) are shown in Figure 4. It can be seen that the addition of PA provided a more violent injection process and a higher flame than the single battery, while the process of PA/SA was almost the same as that of a single battery. A probable reason for violent jetting is that the heat absorption led to a reduction in the internal reaction rate of the battery, active combustibles accumulated inside the battery, and when the temperature reached the onset temperature of thermal runaway, the internal combustibles were instantly released,

leading to a more violent jetting. The t_{com} for Groups II (PA) and III (PA/SA) was 42 and 25 s, respectively, while the t_{com} for a single battery was 10 s. The thermal runaway was thus made more harmful by the addition of PA, whereas the t_{com} of PA/SA reduced by 40.5% compared to that of PA, demonstrating SA's efficiency in inhibiting PA combustion. Both PCM additions provided relatively well-preserved battery shells, as shown by the residue plots. Two potential explanations for this include the fact that PA has a relatively low boiling point and would not cause significant damage to the battery case and that the heat absorption ability of PA prevents the breakdown of the battery case.

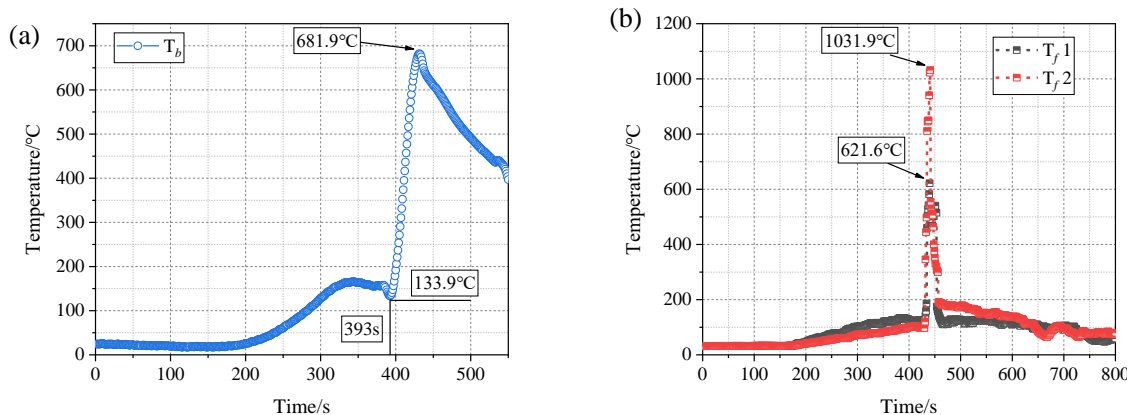


Figure 3. Temperature of Group I: (a) The battery surface temperature; (b) the flame temperature (redrawn from [37]).

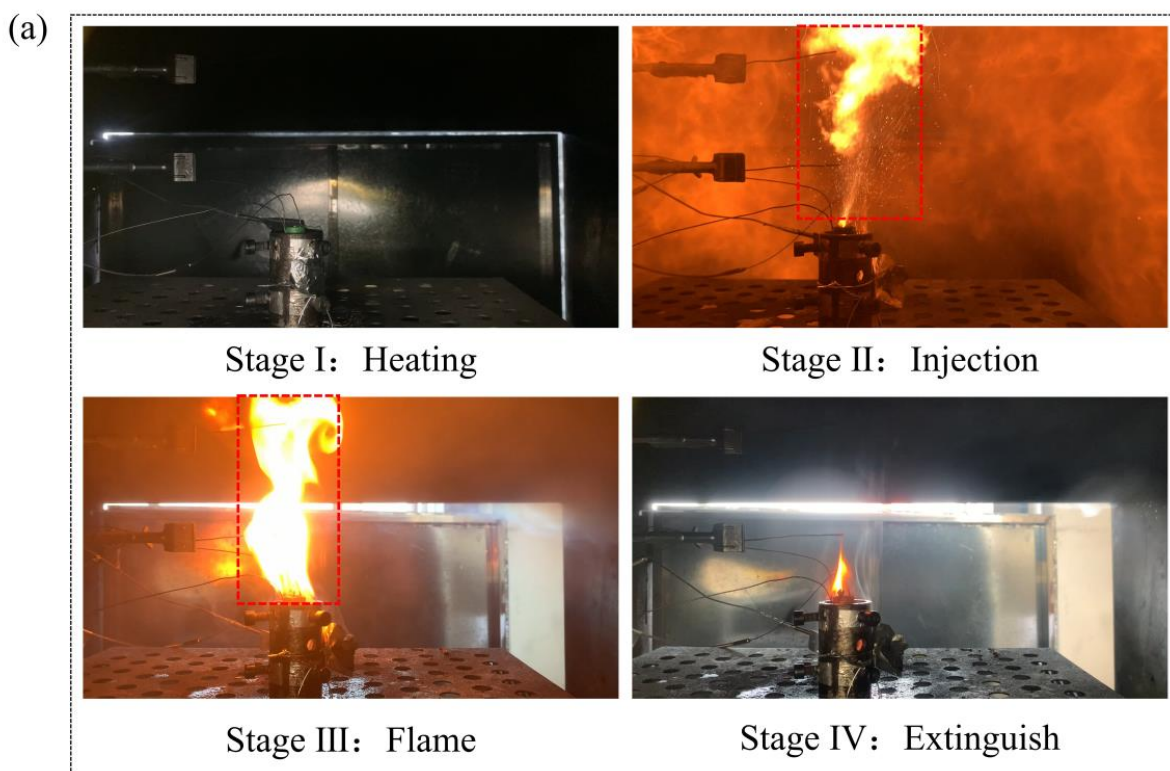


Figure 4. Cont.

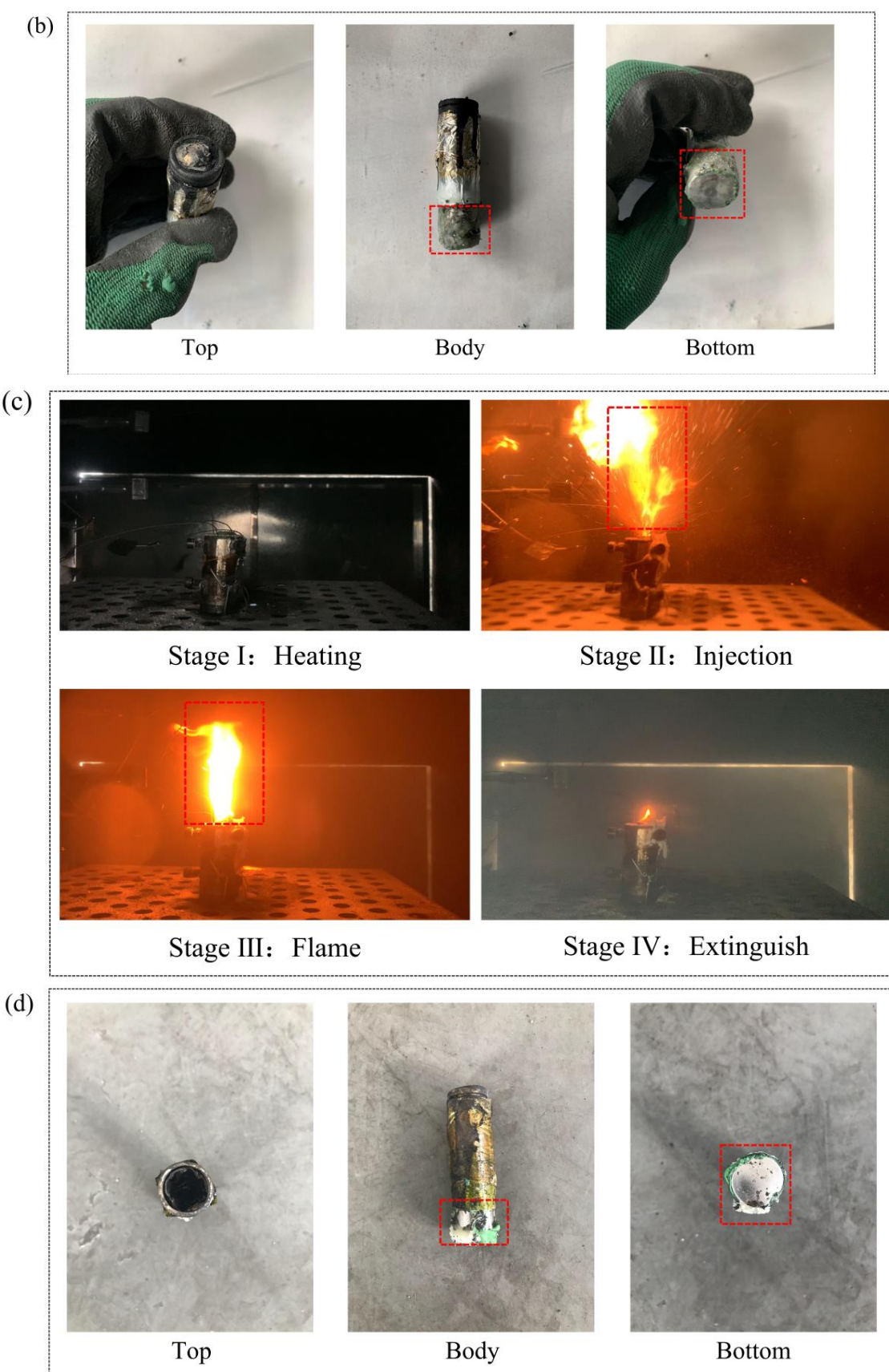


Figure 4. Thermal runaway process and residues of Groups II and III: (a,c) The thermal runaway process of Groups II and III; (b,d) the battery residues of Groups II and III.

Figure 5 shows the battery and flame temperature curves during thermal runaway for both PCMs. According to Figure 5a, the addition of PA increased the thermal runaway onset temperature by 33.5%, while also prolonging the onset time by 58.6%. The $T_{b\text{-max}}$ (maximum value of T_b) of Group II (PA) was 644.9°C , which shows no significant change from the single battery. In comparison to pure PA, the addition of SA substantially delayed the thermal runaway onset time and temperature, with an increase of 6.5% in onset temperature and 47.1% in thermal runaway onset time; the $T_{b\text{-max}}$ dropped by 23.4% as well. The latent heat was calculated based on the properties of the two PCMs in the Materials section, with an ΔH (maximum latent heat absorption) of 1.98 kJ for PA and 3.4 kJ for SA/PA. As a result, the huge latent heat of PA was able to absorb the heat transferred by the heating rod, thus delaying the thermal runaway. The ΔH of SA/PA was increased by 41.7% more than that of PA, which resulted in a substantial increase in the thermal runaway onset time. Figure 5b demonstrates that, despite the prolonged steady combustion duration, PA had little impact on the flame threat, as seen by the tiny difference in the peak battery flame temperature of Groups II (PA) and I (single battery). It is noteworthy that the $T_{f2\text{-max}}$ of PA/SA was significantly increased, related to the fluctuation of the flame during the combustion process, resulting in both a higher T_{f1} and a higher T_{f2} .

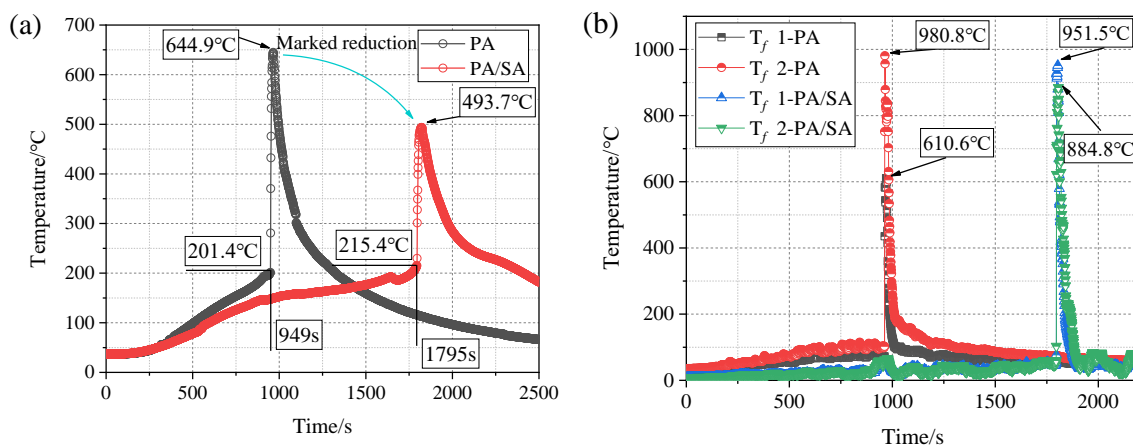


Figure 5. Temperature of Groups II and III: (a) The battery surface temperature; (b) the flame temperature.

The $t_{one\text{-max}}$ (time interval between thermal runaway onset and the maximum temperature) of the three groups is shown in Figure 6. The $t_{one\text{-max}}$ of Group I (single battery) was 39 s, which was the longest among the three groups, while the $t_{one\text{-max}}$ of Group II (PA) was only 16 s, which was reduced by 59%. Therefore, the PA was ignited after the battery thermal runaway, which accelerated the inside chemical reaction and caused the battery temperature to peak more quickly. The $t_{one\text{-max}}$ of Group III (PA/SA) was 37 s, which was 56.8% longer than that of Group II (PA), although slightly shorter than that of Group I (single battery). A significant quantity of heat was absorbed by SA due to its high latent heat, which, on the one hand prevented a temperature rise in the battery and, on the other, hindered the combustion of PA, slowing the battery temperature rise rate. Therefore, the introduction of SA for inhibiting PA combustion was effective and helpful in reducing the rise in battery temperature.

The material temperature of the two PCMs is shown in Figure 7a, indicating that the T_m of PA/SA was much lower than that of PA, which shows that the heat absorption effect of SA greatly lowered the material temperature of the CPCM, with a maximum reduction of 45.8%. The inhibition mechanism of SA is shown in Equations (1) and (2) [38,39]. Because of its enormous latent heat capacity and the contribution of its crystal water to absorb heat, the battery temperature decreased substantially and the thermal runaway onset time was greatly prolonged. Additionally, the concentration of combustibles could be reduced due to the evaporation of crystal water, which also partially prevented the thermal runaway

reaction of the battery. Figure 7b shows the battery $T_{rate-ave}$ (average temperature rise rate) before thermal runaway of the three groups of experiments, and the $T_{rate-ave}$ of Group II (PA) was reduced by 38.0% more than that of Group I (single battery), while the $T_{rate-ave}$ of Group III (PA/SA) was only 0.1 °C/s, which was 87.3% and 44.4% lower than that of the single battery and PA, respectively. Therefore, the excellent heat absorption effect of SA greatly prevented the battery temperature rise, thus prolonging the thermal runaway onset, and SA also had an inhibitory effect on the combustion of PA, which decreased the material's temperature.

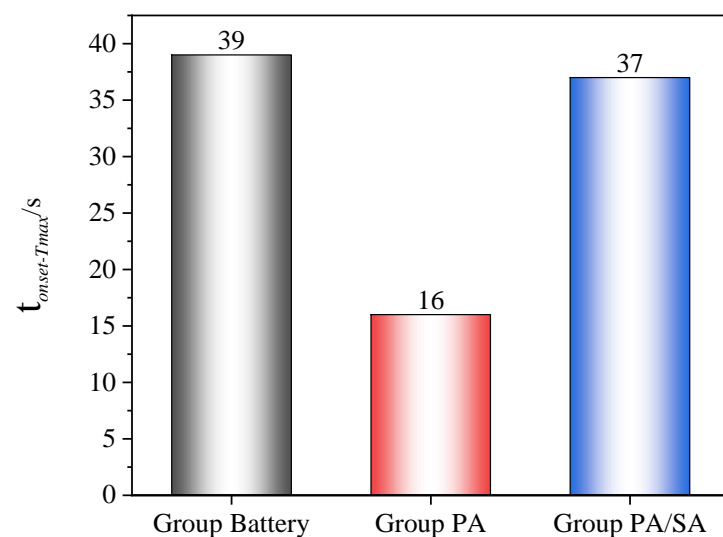
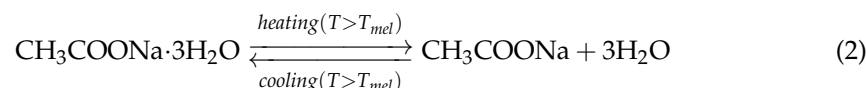


Figure 6. Time of the different groups from thermal runaway onset to maximum temperature of the battery.

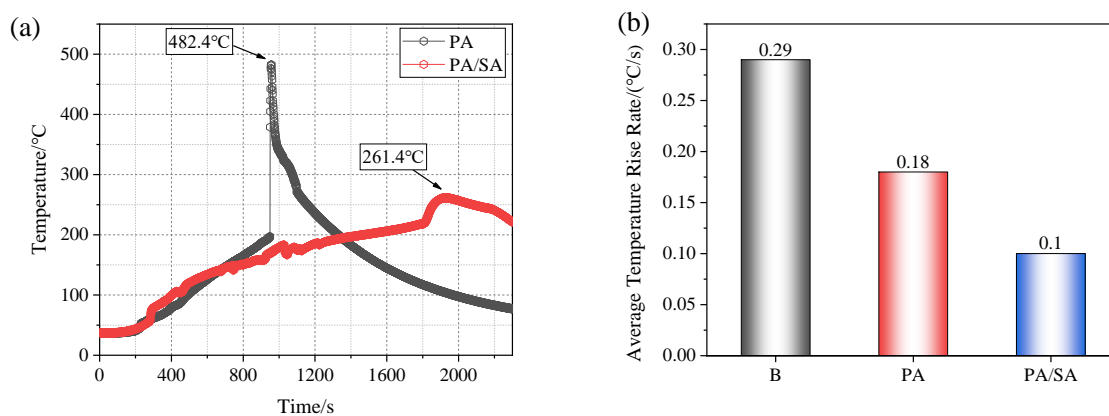


Figure 7. Temperature of the material and battery temperature rise rate of Groups II and III: (a) The material temperature; (b) the battery temperature rise rate before thermal runaway.

3.3. Influence of Heating Power

In actuality, overheating triggers thermal runaway accidents, and the heating power acting on the battery is usually random and variable. Different heating powers lead to variations in the characteristic time and temperature of the battery's thermal runaway,

which may affect the thermal runaway suppression effect of the CPCM. To verify the suitability of the new CPCM at higher heating powers, thermal runaway experiments at a heating power of 500 W are presented in this section. Figure 8 shows the temperature curves of a single battery at 500 W, for which the onset of thermal runaway occurred 21.9% earlier than that at 200 W, while the $T_{b\text{-max}}$ and $T_{f\text{-max}}$ (maximum value of T_f1 or T_f2) did not change significantly. Therefore, the increased heating power merely accelerated the onset time of thermal runaway, with less effect on the battery and flame temperature.

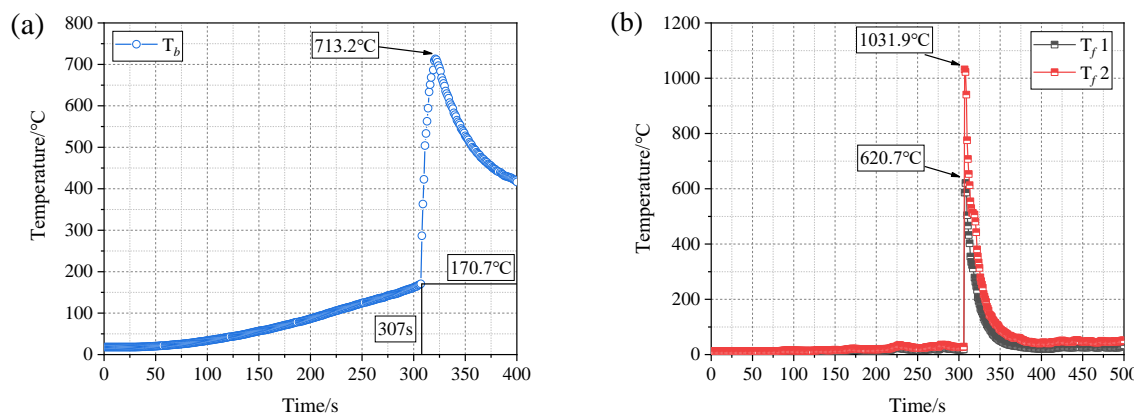


Figure 8. Temperature of Group I at 500 W: (a) The battery surface temperature; (b) the flame temperature.

Figure 9a shows that the thermal runaway onset time of Group II (PA) was 635 s, and the temperature was 215.3 °C. Comparing the results with those in Section 3.2, the thermal runaway onset temperature was less varied, while the thermal runaway onset time was reduced by 33.1%. The thermal runaway onset time was decreased by 54.7% in Group III (PA/SA), which showed a more noticeable difference. Increasing the heating power had little impact on the temperature of the battery or the flame. In addition, it is worth noting that the T_{f2} of the PA/SA at 500 W was significantly lower than that at 200 W. The main reason is that the greater heating power resulted in a more intense internal reaction, and thus the occurrence of a lower flame was greatly reduced.

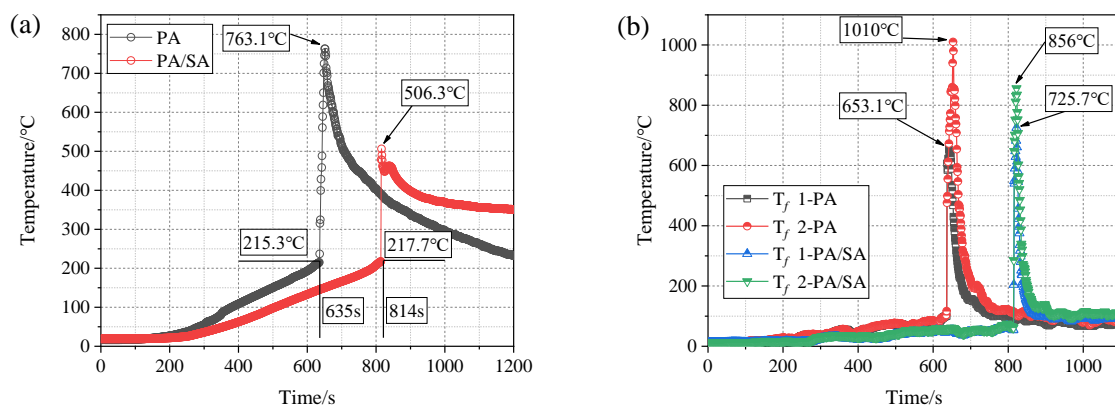


Figure 9. Temperature of Groups II and III at 500 W: (a) The battery surface temperature; (b) the flame temperature.

Figure 10 shows a comparison of the combustion duration and temperature rise rate for two heating powers, highlighting that an increased heating power is a greater threat. As seen in Figure 10a, the t_{com} of the single battery nearly remained unchanged, while that of Group II (PA) increased by 16%, indicating that a higher heating power causes more PA to ignite, leading to a bigger t_{com} . Group III (PA/SA) changed most significantly, with an

increase of 37.5%, indicating that an increased heating power significantly weakens the inhibition of PA combustion by SA. Figure 10b shows that increasing the heating power leads to a rapid increase in the battery temperature, with $T_{rate-ave}$ increasing by 42% for a single battery, and 43.8% and 60% for PA and PA/SA, respectively. An increased heating power thus results in more severe thermal runaway consequences and also diminishes the heat-absorbing capabilities of both PCMs, decreasing the efficiency of thermal runaway retardation.

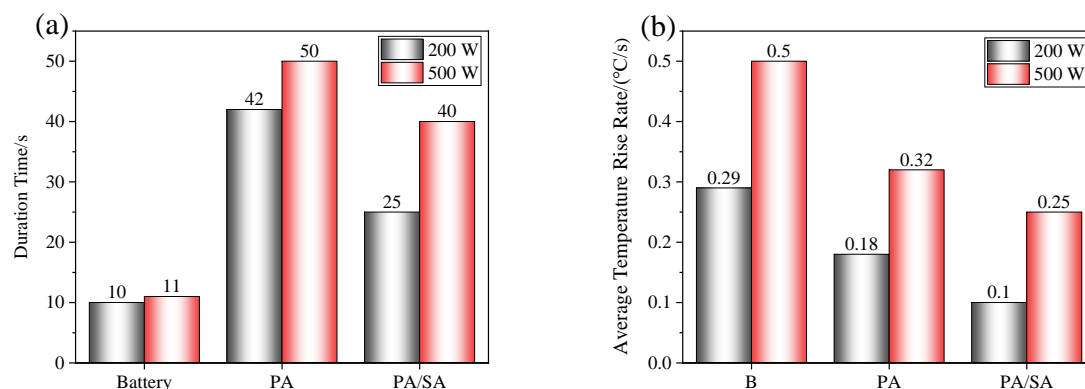


Figure 10. Comparison of two heating powers: (a) Burning duration; (b) battery temperature rise rate before thermal runaway.

Figure 11 shows the comparison of two heating powers after thermal runaway. The temperature of the single battery was significantly affected by the heating power; $t_{one-max}$ dropped by 64.1%, demonstrating that increasing the heating power made the internal reaction rate during thermal runaway faster and caused a slight increase in T_{b-max} , which was unfavorable for suppressing thermal runaway. While the 15.5% increase in T_{b-max} demonstrated that a larger heating power led to a fuller combustion of the PA and the battery, which produced a higher peak temperature of the battery, the unchanged $t_{one-max}$ of Group II (PA) at both heating powers indicates that the accelerating effect of PA combustion on the rise in battery temperature was almost independent of the heating power. It is interesting to note that the $t_{one-max}$ for Group III (PA/SA) was only 2 s, indicating that the increased heating power significantly reduced the inhibition effect of PA/SA on the rise in the battery temperature after thermal runaway, which is also related to the increased heating power and the lower peak temperature of the battery. The T_b of Group III (PA/SA) was the smallest among the three groups, suggesting the efficiency of PA/SA in reducing the battery's peak temperatures, and it was nearly unaffected by the heating power, despite the rapid temperature rise of the battery following thermal runaway under 500 W heating.

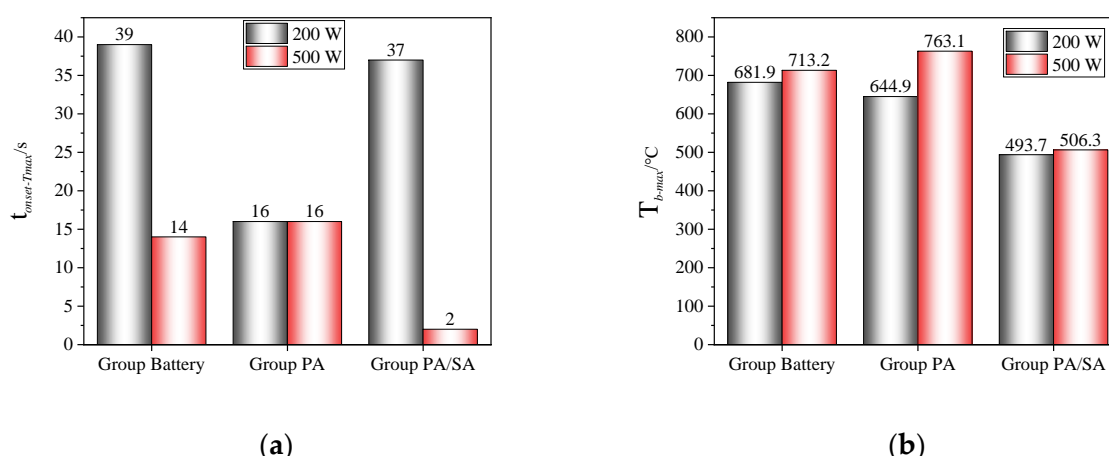


Figure 11. Comparison of two heating powers: (a) $t_{one-max}$; (b) T_{b-max} .

4. Conclusions

To counter the thermal runaway of lithium-ion batteries and to reduce the flammable risk of PA, a new CPCM was proposed with an enhanced heat absorption capability to mitigate thermal runaway and to reduce the threat of PA. Heating rods of the same size as the battery were used to trigger thermal runaway. The combustion process and flame and battery surface temperatures during thermal runaway were recorded, and the thermal runaway mitigation mechanism of the CPCM was revealed. Additionally, comparisons and analyses of the characteristics of thermal runaway and the impact of the PCMs at various heating powers were conducted. The main conclusions of this study are summarized as follows:

- (1) The thermal runaway of the battery was accompanied by violent combustion behaviors and a high temperature. The heat absorption of PA delayed the thermal runaway by 33.5%, but its flammable characteristic led to more violent combustion and a longer combustion duration. The t_{com} of Group II (PA) was 42 s, while that of Group I (single battery) was only 10 s.
- (2) The heat absorption of SA reduced the combustion of PA, and Group III (PA/SA) had a 40.5% reduction in t_{com} than that of Group II (PA). The rise in battery temperature was significantly slowed down by PA/SA, and its $T_{rate-ave}$ was decreased by 87.3% and 44.4% in comparison to PA and a single battery, respectively. The temperature of the battery flame was essentially unaffected by either PCM.
- (3) Although the battery and flame temperatures of the two PCM groups were essentially unaffected by the increasing heating power, the thermal runaway mitigation effect was significantly reduced, while the thermal runaway onset time was advanced by at least 33.1%. The heating power had a pronounced impact on SA/PA, with t_{com} and $T_{rate-ave}$ increasing by 37.5% and 60%, respectively. The fact that the $t_{one-max}$ for Group III (PA/SA) changed from 37 to 2 s further illustrates the tremendous impact of the heating power on the suppression effect of PA/SA on a battery' temperature rise.

Herein, an experimental study was conducted on the effect of PA on the thermal runaway of lithium-ion batteries and a CPCM was proposed for inhibiting the combustion of PA and mitigating the thermal runaway. However, this paper did not conduct a detailed study of different ratios of the CPCM, nor did it conduct experiments to verify its thermal management performance. Therefore, the future work requires an in-depth study of different material ratios and thermal management performance.

Author Contributions: Conceptualization, J.M. and G.S.; methodology, J.M. and H.L.; writing—original draft preparation, J.M.; writing—review and editing, J.M., G.S., H.L. and Z.W. All authors have read and agreed to the published version of the manuscript.

Funding: This research was funded by the National Natural Science Foundation of China (No. 52074279), the National Natural Science Foundation of China (No. 52204253), the Jiangsu Provincial Double-Innovation Doctor Program (No. 140923027), the Opening Foundation of Civil Aircraft Fire Science and Safety Engineering Key Laboratory of Sichuan Province (No. MZ2023KF06), and the Fundamental Research Funds for the Central Universities (No. 2022QN1009).

Data Availability Statement: All data are contained within the article.

Conflicts of Interest: The authors declare no conflict of interest.

References

1. Adnan, M. The Future of Energy Storage: Advancements and Roadmaps for Lithium-Ion Batteries. *Int. J. Mol. Sci.* **2023**, *24*, 7457. [[CrossRef](#)]
2. Li, M.; Lu, J.; Chen, Z.; Amine, K. 30 Years of Lithium-Ion Batteries. *Adv. Mater.* **2018**, *30*, 1800561. [[CrossRef](#)] [[PubMed](#)]
3. Kim, T.; Song, W.; Son, D.-Y.; Ono, L.K.; Qi, Y. Lithium-ion batteries: Outlook on present, future, and hybridized technologies. *J. Mater. Chem. A* **2019**, *7*, 2942–2964. [[CrossRef](#)]
4. Ouyang, D.; Weng, J.; Chen, M.; Wang, J. Impact of high-temperature environment on the optimal cycle rate of lithium-ion battery. *J. Energy Storage* **2020**, *28*, 101242. [[CrossRef](#)]

5. Leng, F.; Tan, C.M.; Pecht, M. Effect of Temperature on the Aging rate of Li Ion Battery Operating above Room Temperature. *Sci. Rep.* **2015**, *5*, 12967. [[CrossRef](#)]
6. Feng, X.; Sun, J.; Ouyang, M.; He, X.; Lu, L.; Han, X.; Fang, M.; Peng, H. Characterization of large format lithium ion battery exposed to extremely high temperature. *J. Power Sources* **2014**, *272*, 457–467. [[CrossRef](#)]
7. Lu, L.; Han, X.; Li, J.; Hua, J.; Ouyang, M. A review on the key issues for lithium-ion battery management in electric vehicles. *J. Power Sources* **2013**, *226*, 272–288. [[CrossRef](#)]
8. Ping, P.; Peng, R.; Kong, D.; Chen, G.; Wen, J. Investigation on thermal management performance of PCM-fin structure for Li-ion battery module in high-temperature environment. *Energy Convers. Manag.* **2018**, *176*, 131–146. [[CrossRef](#)]
9. Liu, J.; Chen, H.; Huang, S.; Jiao, Y.; Chen, M. Recent Progress and Prospects in Liquid Cooling Thermal Management System for Lithium-Ion Batteries. *Batteries* **2023**, *9*, 400. [[CrossRef](#)]
10. Abbas, S.; Ramadan, Z.; Park, C.W. Thermal performance analysis of compact-type simulative battery module with paraffin as phase-change material and flat plate heat pipe. *Int. J. Heat Mass Transf.* **2021**, *173*, 121269. [[CrossRef](#)]
11. An, Z.; Luo, Y.; Zhang, C.; Li, D. Performance of chocolate bar-shaped modular thermal management system combined metal lattice liquid-cooling plate with paraffin in high-rate discharge. *J. Energy Storage* **2022**, *56*, 106017. [[CrossRef](#)]
12. Hussain, A.; Abidi, I.H.; Tso, C.Y.; Chan, K.C.; Luo, Z.; Chao, C.Y.H. Thermal management of lithium ion batteries using graphene coated nickel foam saturated with phase change materials. *Int. J. Therm. Sci.* **2018**, *124*, 23–35. [[CrossRef](#)]
13. Wang, Z.; Du, C.; Qi, R.; Wang, Y. Experimental study on thermal management of lithium-ion battery with graphite powder based composite phase change materials covering the whole climatic range. *Appl. Therm. Eng.* **2022**, *216*, 119072. [[CrossRef](#)]
14. Zhao, Y.; Zou, B.; Ding, J.; Ding, Y. Experimental and numerical investigation of a hybrid battery thermal management system based on copper foam-paraffin composite phase change material and liquid cooling. *Appl. Therm. Eng.* **2023**, *218*, 119312. [[CrossRef](#)]
15. Greco, A.; Jiang, X.; Cao, D. An investigation of lithium-ion battery thermal management using paraffin/porous-graphite-matrix composite. *J. Power Sources* **2015**, *278*, 50–68. [[CrossRef](#)]
16. Kang, W.; Zhao, Y.; Jia, X.; Hao, L.; Dang, L.; Wei, H. Paraffin/SiC as a Novel Composite Phase-Change Material for a Lithium-Ion Battery Thermal Management System. *Trans. Tianjin Univ.* **2021**, *27*, 55–63. [[CrossRef](#)]
17. Wang, S.; Zhang, D.; Li, C.; Wang, J.; Zhang, J.; Cheng, Y.; Mei, W.; Cheng, S.; Qin, P.; Duan, Q.; et al. Numerical optimization for a phase change material based lithium-ion battery thermal management system. *Appl. Therm. Eng.* **2023**, *222*, 119839. [[CrossRef](#)]
18. Chen, M.; Zhang, S.; Zhao, L.; Weng, J.; Ouyang, D.; Chen, Q.; Kong, Q.; Wang, J. Preparation of thermally conductive composite phase change materials and its application in lithium-ion batteries thermal management. *J. Energy Storage* **2022**, *52*, 104857. [[CrossRef](#)]
19. Chen, H.; Abidi, A.; Hussein, A.K.; Younis, O.; Degani, M.; Heidarshenas, B. Investigation of the use of extended surfaces in paraffin wax phase change material in thermal management of a cylindrical lithium-ion battery: Applicable in the aerospace industry. *J. Energy Storage* **2022**, *45*, 103685. [[CrossRef](#)]
20. Mei, J.; Shi, G.; Liu, H.; Wang, Z.; Chen, M. Investigation on the optimization strategy of phase change material thermal management system for lithium-ion battery. *J. Energy Storage* **2022**, *55*, 105365. [[CrossRef](#)]
21. Liu, J.; Wang, Z.; Bai, J.; Gao, T.; Mao, N. Heat generation and thermal runaway mechanisms induced by overcharging of aged lithium-ion battery. *Appl. Therm. Eng.* **2022**, *212*, 118565. [[CrossRef](#)]
22. Liu, J.; Huang, Z.; Sun, J.; Wang, Q. Heat generation and thermal runaway of lithium-ion battery induced by slight overcharging cycling. *J. Power Sources* **2022**, *526*, 231136. [[CrossRef](#)]
23. Mao, N.; Zhang, T.; Wang, Z.; Gadkari, S.; Wang, J.; He, T.; Gao, T.; Cai, Q. Revealing the thermal stability and component heat contribution ratio of overcharged lithium-ion batteries during thermal runaway. *Energy* **2023**, *263*, 125786. [[CrossRef](#)]
24. Hu, J.; Liu, T.; Wang, X.; Wang, Z.; Wu, L. Investigation on thermal runaway of 18,650 lithium ion battery under thermal abuse coupled with charging. *J. Energy Storage* **2022**, *51*, 104482. [[CrossRef](#)]
25. Liu, Z.; Guo, X.; Meng, N.; Yu, Z.; Yang, H. Study of thermal runaway and the combustion behavior of lithium-ion batteries overcharged with high current rates. *Thermochim. Acta* **2022**, *715*, 179276. [[CrossRef](#)]
26. García, A.; Zhao, P.; Monsalve-Serrano, J.; Villalta, D.; Martinez-Boggio, S. Optical diagnostics of the venting spray and combustion behaviour during Li-ion battery thermal runaway induced by ramp heating. *Appl. Therm. Eng.* **2023**, *218*, 119308. [[CrossRef](#)]
27. Golubkov, A.W.; Planteu, R.; Krohn, P.; Rasch, B.; Brunnsteiner, B.; Thaler, A.; Hacker, V. Thermal runaway of large automotive Li-ion batteries. *RSC Adv.* **2018**, *8*, 40172–40186. [[CrossRef](#)]
28. He, C.X.; Yue, Q.L.; Chen, Q.; Zhao, T.S. Modeling thermal runaway of lithium-ion batteries with a venting process. *Appl. Energy* **2022**, *327*, 120110. [[CrossRef](#)]
29. Li, W.; Wang, H.; Zhang, Y.; Ouyang, M. Flammability characteristics of the battery vent gas: A case of NCA and LFP lithium-ion batteries during external heating abuse. *J. Energy Storage* **2019**, *24*, 100775. [[CrossRef](#)]
30. Huang, Z.; Shen, T.; Jin, K.; Sun, J.; Wang, Q. Heating power effect on the thermal runaway characteristics of large-format lithium ion battery with $\text{Li}(\text{Ni}_{1/3}\text{Co}_{1/3}\text{Mn}_{1/3})\text{O}_2$ as cathode. *Energy* **2022**, *239*, 121885. [[CrossRef](#)]
31. Md Said, M.S.; Mohd Tohir, M.Z. Visual and thermal imaging of lithium-ion battery thermal runaway induced by mechanical impact. *J. Loss Prev. Process Ind.* **2022**, *79*, 104854. [[CrossRef](#)]
32. Zhang, W.; Huang, L.; Zhang, Z.; Li, X.; Ma, R.; Ren, Y.; Wu, W. Non-uniform phase change material strategy for directional mitigation of battery thermal runaway propagation. *Renew. Energy* **2022**, *200*, 1338–1351. [[CrossRef](#)]

33. Dai, X.; Kong, D.; Du, J.; Zhang, Y.; Ping, P. Investigation on effect of phase change material on the thermal runaway of lithium-ion battery and exploration of flame retardancy improvement. *Process Saf. Environ. Prot.* **2022**, *159*, 232–242. [[CrossRef](#)]
34. Weng, J.; Ouyang, D.; Yang, X.; Chen, M.; Zhang, G.; Wang, J. Alleviation of thermal runaway propagation in thermal management modules using aerogel felt coupled with flame-retarded phase change material. *Energy Convers. Manag.* **2019**, *200*, 112071. [[CrossRef](#)]
35. Huang, Q.; Li, X.; Zhang, G.; Weng, J.; Wang, Y.; Deng, J. Innovative thermal management and thermal runaway suppression for battery module with flame retardant flexible composite phase change material. *J. Clean. Prod.* **2022**, *330*, 129718. [[CrossRef](#)]
36. Wang, Z.; Wang, J. Investigation of external heating-induced failure propagation behaviors in large-size cell modules with different phase change materials. *Energy* **2020**, *204*, 117946. [[CrossRef](#)]
37. Mei, J.; Shi, G.; Liu, H.; Wang, Z.; Chen, M. Experimental study on the effect of passive retardation method for thermal runaway mitigation of lithium-ion battery. *Appl. Therm. Eng.* **2023**, *230*, 120861. [[CrossRef](#)]
38. Wang, Y.; Yu, K.; Peng, H.; Ling, X. Preparation and thermal properties of sodium acetate trihydrate as a novel phase change material for energy storage. *Energy* **2019**, *167*, 269–274. [[CrossRef](#)]
39. Hu, P.; Lu, D.-J.; Fan, X.-Y.; Zhou, X.; Chen, Z.-S. Phase change performance of sodium acetate trihydrate with AlN nanoparticles and CMC. *Sol. Energy Mater. Sol. Cells* **2011**, *95*, 2645–2649. [[CrossRef](#)]

Disclaimer/Publisher's Note: The statements, opinions and data contained in all publications are solely those of the individual author(s) and contributor(s) and not of MDPI and/or the editor(s). MDPI and/or the editor(s) disclaim responsibility for any injury to people or property resulting from any ideas, methods, instructions or products referred to in the content.